IEEE Access
Multidisciplinary | Rapid Review | Open Access Journal

Received 13 April 2024, accepted 9 May 2024, date of publication 14 May 2024, date of current version 21 May 2024.

Digital Object Identifier 10.1109/ACCESS.2024.3400997

METHODS

Two Patch Antennas for Two- or Four-OAM-Mode Generation

DANDAN LIU[1], QINQIN SUN[2], AND WEI WU[1]
[1]College of Weapons Engineering, Naval University of Engineering, Wuhan 430074, China
[2]Wuhan Maritime Communication Research Institute, Wuhan 430200, China

Corresponding author: Dandan Liu (liudandan_nue@126.com)

This work was supported in part by the National Natural Science Foundation of China (NSFC) under Grant 62073334, and in part by the Independent Project of the Naval University of Engineering under Grant 2022507070.

ABSTRACT Two patch antennas that can generate two or four orbital angular momentum (OAM) modes are designed and verified to work at frequency band from 2.2GHz to 2.7GHz. One antenna is composed of two single OAM mode monopole patch antenna systems with one common ground plane and it can generate two OAM modes: mode l=1 and mode l=−1. This antenna is designed, simulated, fabricated and tested. Its reflection coefficients, radiation patterns, phase distributions and isolation between two different OAM mode channels are obtained. Phase distributions of the two OAM modes are measured to show the effectiveness of the antenna to generate two OAM modes. Channel isolation between these two OAM modes is 25.72dB at 2.598GHz and more than 15dB at the frequency band from 2.585GHz to 2.62GHz. The measurement results have shown that this two-OAM-mode antenna can produce two isolated channels at the same frequency band. Another monopole patch antenna has been designed and verified by simulation to be able to generate four OAM modes. This four-OAM-mode antenna provides an example that this kind of multiplexed monopole patch antennas can multiplex more OAM modes together.

INDEX TERMS Orbital angular momentum (OAM), multiple OAM modes, multiplexed antenna, feeding network.

I. INTRODUCTION

Orbital angular momentum (OAM) is one of the basic physical properties of electromagnetic (EM) waves [1], where EM waves have a phase factor of $e^{il\varphi}$, and l is called OAM mode. OAM waves have spiral wave fronts along the propagation direction [2]. Due to the characteristics of OAM, waves with different OAM modes are orthogonal to each other [3]. Thus, OAM can be used as a new degree of freedom in communications to improve channel capacity. OAM has attracted attention of researchers after Allen et. al demonstrated Laguerre Gaussian (LG) spiral light waves can have OAM in [4]. In 2007, OAM waves in EM field have been realized by simulation for the first time in [5]. Since then many approaches have been proposed to generate OAM waves, such as: reflecting surface approach [6], [7], [8], transmission surface approach [9], [10], [11], dielectric resonator [12], [13], cavity [14], [15], [16], single patch antenna [17], [18] and antenna array [19], [20], [21], [22].

To make OAM technology be more useful in communication systems, it is desirable to design antennas with multiple OAM modes. A dual OAM modes (l=3,−3) antenna, based on the method of traveling-wave loop antenna, is proposed to transmit different message at the same frequency band [16]. A multiplexed three OAM modes (l=−1, 0, 1) antenna, composed of an open-ended rectangular waveguide matrix feed, an OAM mode mux and a Cassegrain dual-reflector, is also presented [23]. These two antenna systems, which have the structure of cavity, are effective to produce multiple OAM modes. Another antenna is proposed to have a planar structure and generate two OAM modes (l =−1, 1) in [24]. It can be concluded that the antenna has complex structure when more OAM modes are multiplexed.

In this paper, two planar antennas with simple principle and structure are proposed to generate two or four OAM modes. The antennas are based on the method of phased antenna

The associate editor coordinating the review of this manuscript and approving it for publication was Pavlos I. Lazaridis.

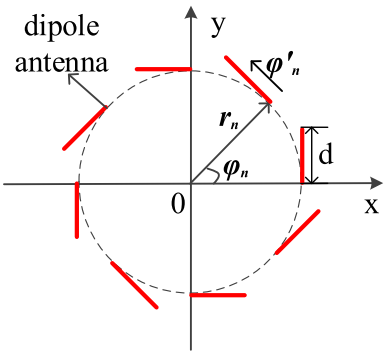

FIGURE 1. Geometry of the azimuthal antenna array.

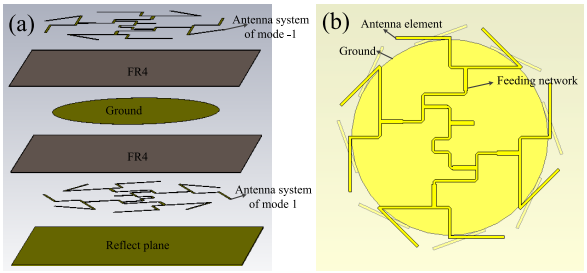

FIGURE 2. Geometry of the two-OAM-mode antenna system. (a) Explosive view; (b) Top view.

array. The two-OAM-mode antenna is composed of two OAM antenna arrays, two feeding networks and one common ground. Reflection parameters, radiation patterns, phase distributions and transmission coefficients of this antenna are measured. The comparison between the simulation and measurement results has verified the effectiveness of the proposed antenna system in generating two OAM waves. The test results of isolation shows that the proposed antenna can work well in different OAM mode channels. A four-OAM-mode antenna is then designed and simulated as an evidence that planer antennas can multiplex more than two OAM modes. This antenna is composed of four OAM antenna arrays, four feeding networks and three common grounds. Simulation results have shown that this antenna can generate four OAM modes successfully.

II. DESIGN AND VERIFICATION OF A TWO-OAM-MODE ANTENNA

In this section, structure of the proposed antenna is presented. Reflection coefficients, radiation patterns, phase distributions and channel isolation of two-OAM-mode antenna are tested.

A. DESIGN OF THE PROPOSED ANTENNA

As shown in Figure 1, antenna elements are rotated around the center of the proposed antenna. The current distribution of the nth antenna element is $\boldsymbol{I} = \boldsymbol{\varphi'_n} e^{il\varphi_n}$, where $\boldsymbol{\varphi'_n}$ is the unit direction vector, $\varphi_n = 2\pi n/N$, and N is the total number of the antenna array.

The E-field of the azimuthal dipole antenna array is $\boldsymbol{E}$, as displayed in equation (1) [25].

$$\begin{aligned}
\boldsymbol{E} = &-\frac{i^l N\mu\omega d}{16\pi r} e^{-ikr}\{J_{(l-1)}(ka\sin\theta) \\
&\times [(\boldsymbol{x} - e^{i\frac{\pi}{2}}\boldsymbol{y})(\cos^2\theta - 1)e^{i(l+1)\varphi} \\
&+ (\boldsymbol{x} + e^{i\frac{\pi}{2}}\boldsymbol{y})(\cos^2\theta + 1)e^{i(l-1)\varphi} - 2\boldsymbol{z}\sin\theta e^{il\varphi}] \\
&+ J_{(l+1)}(ka\sin\theta)[(\boldsymbol{x} - e^{i\frac{\pi}{2}}\boldsymbol{y})(\cos^2\theta + 1)e^{i(l+1)\varphi} \\
&+ (\boldsymbol{x} + e^{i\frac{\pi}{2}}\boldsymbol{y})(\cos^2\theta - 1)e^{i(l-1)\varphi} - 2\boldsymbol{z}\sin\theta e^{il\varphi}]\} \\
= &-\frac{i^l N\mu\omega d}{16\pi r} e^{-ikr}\{(\boldsymbol{x} - e^{i\frac{\pi}{2}}\boldsymbol{y})e^{i(l+1)\varphi} \\
&\times [(\cos^2\theta - 1)J_{(l-1)}(ka\sin\theta) \\
&+ (\cos^2\theta + 1)J_{(l+1)}(ka\sin\theta)] \\
&+ (\boldsymbol{x} + e^{i\frac{\pi}{2}}\boldsymbol{y})e^{i(l-1)\varphi}[(\cos^2\theta + 1)J_{(l-1)}(ka\sin\theta) \\
&+ (\cos^2\theta - 1)J_{(l+1)}(ka\sin\theta)] \\
&- 2\boldsymbol{z}\sin\theta e^{il\varphi}[J_{(l-1)}(ka\sin\theta) + J_{(l+1)}(ka\sin\theta)]\} \quad (1)
\end{aligned}$$

$\boldsymbol{E}$ has complicated composition structure. There are two intrinsic rotations (spin angular momentum, SAM): $(\boldsymbol{x} - e^{i\frac{\pi}{2}}\boldsymbol{y})$ and $(\boldsymbol{x} + e^{i\frac{\pi}{2}}\boldsymbol{y})$, which correspond to polarization [26], [27]. These polarizations, which the $\boldsymbol{x}$ component has a forward or backward phase delay $\pi/2$ compared to the $\boldsymbol{y}$ component, are inherently existed in the $\boldsymbol{E}$. The OAM carried by the $\boldsymbol{E}$ are $e^{i(l+1)\varphi}$, $e^{i(l-1)\varphi}$ and $e^{il\varphi}$, which have extrinsic rotations. The extrinsic rotations are related to space. The phase distributions of OAM modes, which change $2\pi l$ on a circle, are reflected on a plane perpendicular to the transmission direction.

Compared with the same direction antenna array, the E-field of a rotated antenna array has different OAM characteristics. Firstly, the $\boldsymbol{z}$ component carries the pure OAM mode. OAM waves with phase factor $e^{il\varphi}$ are orthogonal to each other under different values of l. Thus, the $\boldsymbol{z}$ component is employed when the proposed antenna is used to transmit information. Secondly, radiation patterns of OAM mode 1 and mode -1 do not have a null zone as radiation pattern of the same direction antenna array's OAM mode 0 does. When l is the same, the E-field of the rotated antenna array takes Bessel functions $J_{(l-1)}(ka\sin\theta)$ and $J_{(l+1)}(ka\sin\theta)$, while the Bessel function $J_l(ka\sin\theta)$ is equipped by the E-field generated by the same direction antenna. Thus, the third different characteristics is that this kind of OAM waves will have a smaller null zone and therefore show a better performance in the transmission distance than a same direction antenna array under the same OAM mode.

In this paper, the rotated monopole antenna array is employed to radiate OAM waves. The two-OAM-mode multiplexed antenna system is exhibited in Figure 2.

It can be seen from Figure 2 (a) that the proposed antenna has two antenna systems of mode 1 and -1, two substrates made of FR4, one common ground plane and one reflect plane. The antenna system of mode -1 is on the first layer and the antenna system of mode 1 is on the last layer of the proposed antenna.The antenna system of mode 1 is

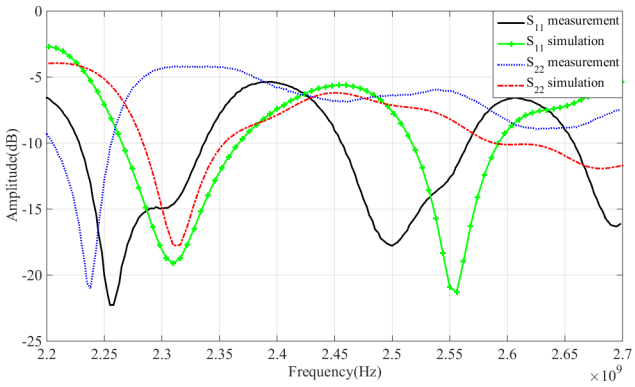

FIGURE 3. Simulation and measurement results of reflection coefficients (S_{11}).

composed of feeding network and a monopole antenna array. The feeding network is constructed by T type junction power distributors and microstrip lines. The monopole antenna array has double side radiation. The feeding network of mode 1 gives phase delay of 45 degree, which is obtained by length difference $\lambda/8$ of microstrip lines, to the antenna array. And the feeding network of mode -1 is obtained by mirroring rotation the feeding network of mode 1. These two different OAM modes antenna systems have a common ground plane, which just covers the feeding networks. Two substrates are made of FR4, which has the permittivity of 4.4 and the height of 0.5 mm. In order to increase the radiation power, a metal reflect plane, which is placed below the proposed antenna, is employed. The size of the proposed antenna is 16 cm$\times$16 cm. The needed OAM mode will be generated when the chosen antenna system is fed.

B. S_{11} SIMULATION AND TEST

Reflection coefficients (S_{11} and S_{22}) need to be tested to verify the working frequency of the proposed antenna. The proposed antenna is designed at 2.4 GHz. But from the simulation result of feeding networks, it is discovered that the proposed antenna can work at frequency band from 2.2 GHz-2.7 GHz. So reflection coefficients of OAM mode 1 and OAM mode -1 are measured at this frequency band (as shown in Figure 3). The black solid line and the green plus line are measurement and simulation S_{11} of OAM mode 1, respectively. The blue dotted line and the red dashed line are the measurement and simulation S_{22} of OAM mode -1. It can be seen that, reflection coefficients of mode 1 and mode -1 have frequency shifting of 50 MHz and 70 MHz, respectively. The difference between simulation and measurement is mainly caused by differences in the thickness and dielectric constant of the dielectric substrate during processing. But the tendency of simulation and measurement results are similar.

C. ANTENNA PATTERN SIMULATION AND TEST

Radiation patterns of the proposed antenna are measured as shown in Figure 4. Horn antenna is the receiving antenna

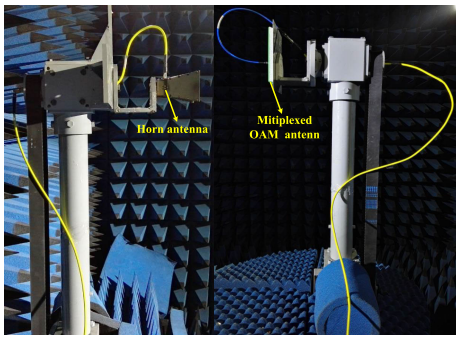

FIGURE 4. Measurement scheme of radiation pattern.

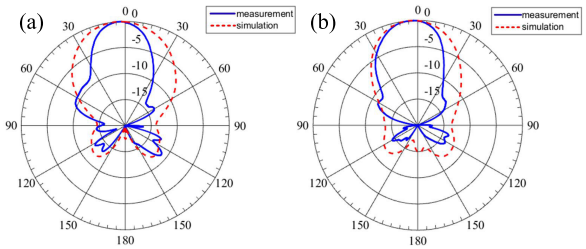

FIGURE 5. Simulation and measurement results of radiation pattern: (a) $l=-1$; (b) $l=1$.

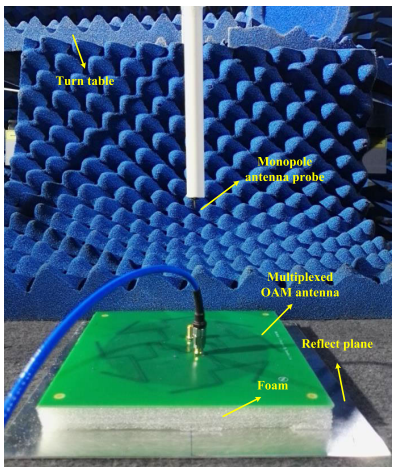

FIGURE 6. Measurement scheme of phase distribution.

and the proposed antenna is the transmitting antenna. When the OAM antenna rotates 360 degree, the horn antenna can receive powers of whole plane of the transmitting antenna. Then the radiation pattern of this plane can be measured. Figure 5 (a) and Figure 5 (b) are simulation and measurement results of normalized radiation patterns for OAM mode -1 and OAM mode 1, respectively.

The measurement results of the radiation patterns are a little thinner than the simulation results. Besides, compared with the simulation results, the measured radiation patterns are not so regular. The difference between simulation and measurement is caused by the manufacture error and the measurement error. But it can be observed that radiation patterns of simulation and measurement are in good agreement.

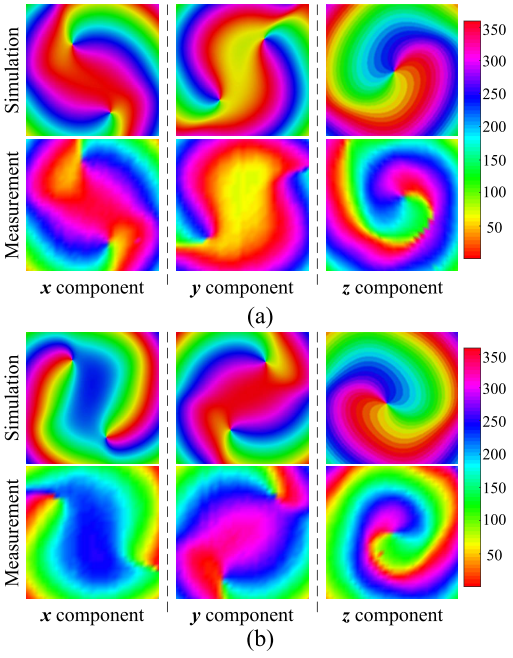

FIGURE 7. Simulation and measurement results of phase distribution in near field: (a) simulated and measured phase of $l=-1$; (b) simulated and measured phase of $l=1$.

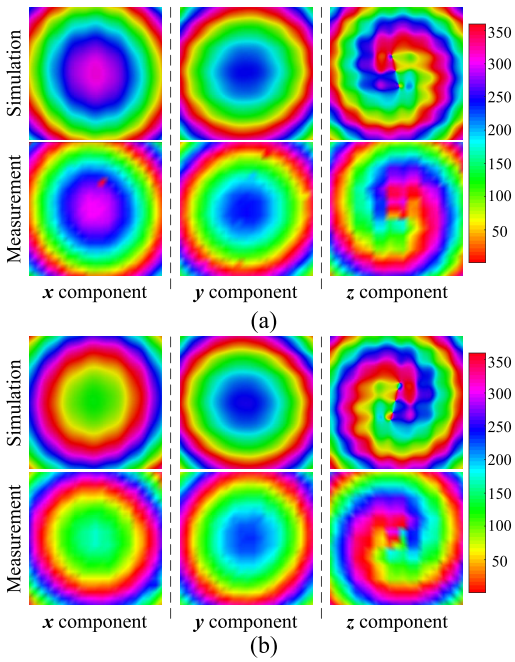

FIGURE 8. Simulation and measurement results of phase distribution in near field: (a) simulated and measured phase of $l=-1$; (b) simulated and measured phase of $l=1$.

D. PHASE DISTRIBUTION SIMULATION AND TEST

In order to verify the proposed antenna's effectiveness in generating OAM waves, phase distributions need to be tested. As shown in Figure 6, a monopole antenna probe is perpendicularly placed above the proposed antenna.

The monopole probe antenna will receive component of electric field (E-field) parallel to itself, so $\boldsymbol{x}$ component, $\boldsymbol{y}$ component and $\boldsymbol{z}$ component of the E-field can be tested by replacing the monopole probe antenna. To clarify the characteristics of the designed antenna, the phase distributions of the E-field are measured in near and far field. The scale of test plane, which is parallel to the proposed antenna, is 30 cm×30 cm and 10 cm far from the OAM antenna in the near field. The probe antenna will move along this plane by step of 1 cm, which can be controlled by computer. Phases of the E-field are tested by vector network analyzer and recorded by computer at each point. From the test results, phases of 900 points can be calculated and are drawn by Matlab.

When $l = -1$, the $\boldsymbol{x}$ component and $\boldsymbol{y}$ component of the E-field do not exhibit obvious OAM characteristics, as shown in Figure 7 (a). The $\boldsymbol{z}$ component displays typical OAM mode -1's phase distribution. From equation (1), it is clear that the $\boldsymbol{x}$ component carries factor $e^{i0\varphi}[(\cos^2\theta - 1)J_{-2}(ka\sin\theta) + (\cos^2\theta + 1)J_0(ka\sin\theta)] + e^{-i2\varphi}[(\cos^2\theta + 1)J_{-2}(ka\sin\theta) + (\cos^2\theta - 1)J_0(ka\sin\theta)]$. The $\boldsymbol{y}$ component equips factor $-e^{i0\varphi}[(\cos^2\theta - 1)J_{-2}(ka\sin\theta) + (\cos^2\theta + 1)J_0(ka\sin\theta)] + e^{-i2\varphi}[(\cos^2\theta + 1)J_{-2}(ka\sin\theta) + (\cos^2\theta - 1)J_0(ka\sin\theta)]$. The factor $\sin\theta e^{-i\varphi}[J_{-2}(ka\sin\theta) + J_0(ka\sin\theta)]$ is taken by the $\boldsymbol{z}$ component. In the test domain, the maximum and minimum value of $\cos^2\theta$ are 1 and 0.38, respectively. Thus, OAM mode 0 and OAM mode -2 are both affect the phase distribution. Therefore, the $\boldsymbol{x}$ component and $\boldsymbol{y}$ component do not show clear phase distribution characteristics. The $\boldsymbol{z}$ component exhibits OAM mode -1's phase distribution.

When $l = 1$, the $\boldsymbol{x}$ component and $\boldsymbol{y}$ component do not show normal OAM characteristics. Only the $\boldsymbol{z}$ component exhibit OAM mode 1's phase distribution, as displayed in Figure 7 (b). The reason is similar to Figure 7 (a).

When the E-field is measured in the far field, the test scan is 100 cm×100 cm large and 140 cm far from the OAM antenna. In this plane, the scale of $\cos^2\theta$ is from 0.89 to 1. When $l = -1$, the factor carried by the $\boldsymbol{x}$ component can be approximately simplified as $e^{i0\varphi}(\cos^2\theta + 1)J_0(ka\sin\theta) + e^{-i2\varphi}(\cos^2\theta + 1)J_{-2}(ka\sin\theta)$. Furthermore, $J_0(ka\sin\theta)$ is much larger than $J_{-2}(ka\sin\theta)$ in this measurement range. Therefore, the $\boldsymbol{x}$ component can be seen as only taking one factor $e^{i0\varphi}(\cos^2\theta + 1)J_0(ka\sin\theta)$. Besides, the $\boldsymbol{y}$ component can also be regarded as equipping one factor $-e^{i0\varphi}(\cos^2\theta + 1)J_0(ka\sin\theta)$. Thus, the $\boldsymbol{x}$ component, $\boldsymbol{y}$ component and $\boldsymbol{z}$ component show OAM characteristics of 0, 0 and -1, respectively, as shown in Figure 8 (a). In Figure 8 (b), phase distributions of OAM mode 0, 0 and 1 are exhibited in the $\boldsymbol{x}$ component, $\boldsymbol{y}$ component and $\boldsymbol{z}$ component, respectively. However, only the $\boldsymbol{z}$ component carries pure OAM mode. Thus, the proposed antenna is considered to radiate OAM modes -1 and 1.

From Figure 7 and Figure 8, it can be seen that the simulation and measurement results of the designed antenna's phase distributions are in good agreement. A conclusion can

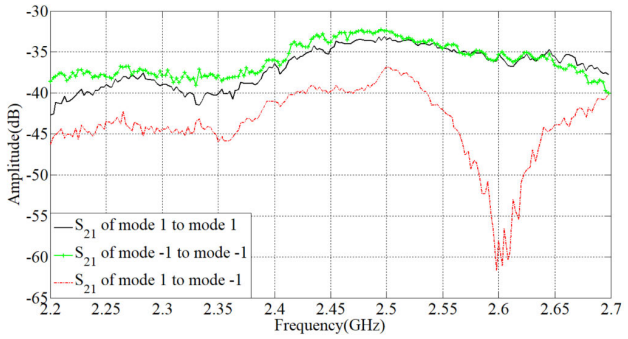

FIGURE 9. Measurement transmission coefficients.

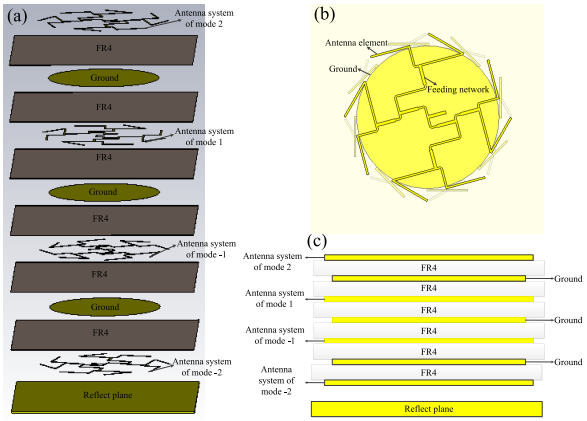

FIGURE 10. Geometry of the four-OAM-mode antenna system. (a) Explosive view; (b) Top view; (c) Side view.

be drawn that the proposed antenna is capable of generating two OAM modes waves.

E. CHANNEL ISOLATION MEASUREMENT

To demonstrate that the proposed antenna can be used in communications, isolation between two channels (mode 1 and mode −1) should be tested. There are two proposed antennas at transmitting terminal and receiving terminal, respectively. Measurement results are displayed in Figure 9. Measured S_{21} of channel mode 1 to mode 1 (green plus line) and mode −1 to mode −1 (black solid line) are transmission coefficients of these two channels and measured S_{21} of channel mode 1 to mode −1 (red dashed line) is the isolation between these two channels. It can be seen that transmission coefficients of mode 1 to mode 1 and mode −1 to mode −1 are approximate −35 dB at frequency band of 2.585 GHz to 2.62 GHz. The isolation between two different OAM mode channels achieves 25.72 dB at 2.598 GHz and is more than 15 dB at the frequency band of 2.585 GHz to 2.62 GHz. In other frequency bands, the isolation level is around 5 dB. Thus, the proposed OAM antenna is recommended to operate in frequency band of 2.585 GHz to 2.62 GHz. These experiment results have demonstrated that the proposed antenna can transmit two signals simultaneously and that these two signals can be divided by the proposed antenna itself at the receiving terminal.

III. DESIGN AND SIMULATION OF A FOUR-OAM-MODE ANTENNA

The antenna proposed in this paper can not only be used in producing two OAM modes but also be employed in generating more than two OAM modes. So the four-OAM-mode antenna is designed in this section, as shown in Figure 10.

Four antenna systems of OAM modes ±1, ±2, six substrates, three ground planes and one reflect plane compose the four-OAM-mode antenna. Antenna systems of OAM modes ±2, whose feeding networks are formed by microtrip lines, are placed on the first and last layers of the proposed antenna. Antenna systems of OAM modes ±1, whose feeding networks are made by striplines, are placed on the third and fifth layers of the proposed antenna. The final ultimate

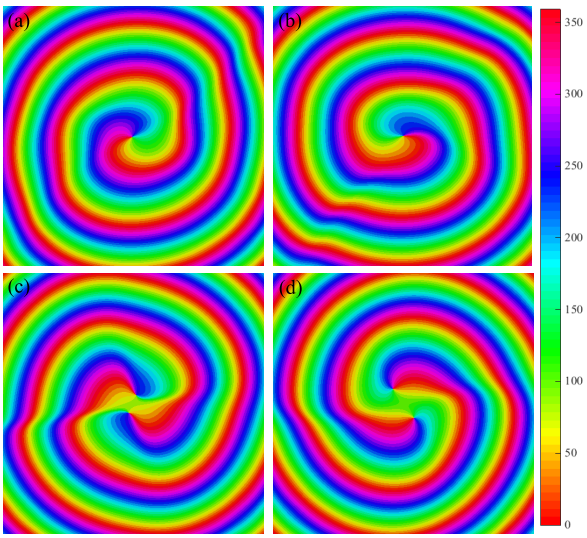

FIGURE 11. Simulation results of phase distribution of four OAM mode. (a) l=1; (b) l=−1; (c) l=2; (d) l=−2.

structure of this four-OAM-mode antenna has seven layers and one reflect plane (see in Figure 10).

Simulation results of the four-OAM-mode antenna are shown in Figure 11 and Figure 12. Figure 11 (a), (b), (c) and (d) are phase distributions of OAM modes $l = \pm 1$ and $l = \pm 2$, respectively. The results display that four OAM modes −2, −1, 1 and 2 are radiated by the designed antenna. Figure 12 exhibits the radiation patterns of the proposed antenna. The red dotted line represents the radiation pattern of mode 1, the blue dotted line stands for the radiation pattern of mode −1, the green solid line shows the radiation pattern of mode 2 and the purple dashed line denotes the radiation patter of mode −2. It can be seen that radiation patterns of mode 1 and mode −1, which do not have the null zone in the radiated center, are similar, and radiation patterns of mode 2 and mode −2, which have the null zone in the radiated center, are similar, too.

From the phase distributions and the radiation patterns of four OAM modes, it can be said that the proposed

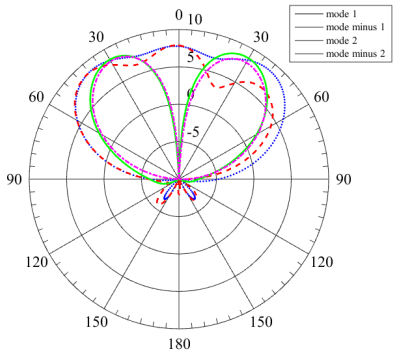

FIGURE 12. Simulation results of radiation of four OAM modes l=±1, ±2.

antenna can successfully produce four OAM modes. So this kind of antenna can be used in generating numerous OAM modes, which need to add more multilayers in the proposed antenna.

IV. CONCLUSION

Two antenna systems composed of single OAM mode antenna systems and common grounds, are presented in this paper. The antennas are rotated antenna arrays. A two-OAM-mode antenna has been simulated, fabricated and measured. Its reflection coefficients have similar tendency but little frequency shifting between simulation and measurement results. The phase distributions demonstrate the effectiveness of the proposed antenna in generating dual OAM modes of ±1. Its radiation patterns are in good agreement between simulation and measurement results. The isolation between two different OAM mode channels is more than 15 dB at the frequency band of 2.585 GHz to 2.62 GHz and reaches 25.72 dB at 2.598 GHz. The test of isolation can prove that the proposed antenna can transmit different signals at the same frequency band. A four-OAM-mode antenna is designed and simulated. This antenna can produce four OAM modes of ±1 and ±2. This kind of antennas can generate multiplexed OAM modes.

REFERENCES

[1] J. D. Jackson, *Classical Electrodynamics*. New York, NY, USA: Wiley, 1962.

[2] L. Allen and M. J. Padgett, "The Poynting vector in Laguerre–Gaussian beams and the interpretation of their angular momentum density," *Opt. Commun.*, vol. 184, no. 1, pp. 67–71, 2000.

[3] J. Sjöholm and K. Palmer, *Angular Momentum of Electromagnetic Radiation*. Sweden: Uppsale Univ., 2007.

[4] L. Allen, M. W. Beijersbergen, R. J. C. Spreeuw, and J. P. Woerdman, "Orbital angular momentum of light and the transformation of Laguerre–Gaussian laser modes," *Phys. Rev. A, Gen. Phys.*, vol. 45, no. 11, pp. 8185–8189, Jun. 1992.

[5] B. Thidé, H. Then, J. Sjöholm, K. Palmer, J. Bergman, T. D. Carozzi, Y. N. Istomin, N. H. Ibragimov, and R. Khamitova, "Utilization of photon orbital angular momentum in the low-frequency radio domain," *Phys. Rev. Lett.*, vol. 99, no. 8, Aug. 2007, Art. no. 087701.

[6] Z.-Y. Yu, Y.-H. Zhang, and H.-T. Gao, "A high-efficiency and broadband folded reflectarray based on an anisotropic metasurface for generating orbital angular momentum vortex beams," *IEEE Access*, vol. 9, pp. 87360–87369, 2021.

[7] H. Liu, H. Xue, Y. Liu, Q. Feng, and L. Li, "Generation of high-order Bessel orbital angular momentum vortex beam using a single-layer reflective metasurface," *IEEE Access*, vol. 8, pp. 126504–126510, 2020.

[8] Z. Wang, X. Pan, F. Yang, S. Xu, M. Li, and D. Su, "Design, analysis, and experiment on high-performance orbital angular momentum beam based on 1-Bit programmable metasurface," *IEEE Access*, vol. 9, pp. 18585–18596, 2021.

[9] Y. Li, S. Li, S.-W. Wong, and B. Liu, "Analysis of OAM performance using metalenses of different resolutions," *IEEE Access*, vol. 9, pp. 66982–66988, 2021.

[10] Y. Ran, T. Cai, L. Shi, J. Wang, J. Liang, S. Wu, J. Li, and Y. Liu, "High-performance transmissive broadband vortex beam generator based on pancharatnam–berry metasurface," *IEEE Access*, vol. 8, pp. 111802–111810, 2020.

[11] O. Edfors and A. J. Johansson, "Is orbital angular momentum (OAM) based radio communication an unexploited area?" *IEEE Trans. Antennas Propag.*, vol. 60, no. 2, pp. 1126–1131, 2012.

[12] J. Liang and S. Zhang, "Orbital angular momentum (OAM) generation by cylinder dielectric resonator antenna for future wireless communications," *IEEE Access*, vol. 4, pp. 9570–9574, 2016.

[13] Z. Yu, N. Guo, and J. Fan, "Water spiral dielectric resonator antenna for generating multimode OAM," *IEEE Antennas Wireless Propag. Lett.*, vol. 19, pp. 601–605, 2020.

[14] W. Zhang, S. Zheng, X. Hui, Y. Chen, X. Jin, H. Chi, and X. Zhang, "Four-OAM-Mode antenna with traveling-wave ring-slot structure," *IEEE Antennas Wireless Propag. Lett.*, vol. 16, pp. 194–197, 2017.

[15] S. Zheng, X. Hui, X. Jin, H. Chi, and X. Zhang, "Transmission characteristics of a twisted radio wave based on circular traveling-wave antenna," *IEEE Trans. Antennas Propag.*, vol. 63, no. 4, pp. 1530–1536, 2015.

[16] X. Hui, S. Zheng, Y. Chen, Y. Hu, X. Jin, H. Chi, and X. Zhang, "Multiplexed millimeter wave communication with dual orbital angular momentum (OAM) mode antennas," *Sci. Rep.*, vol. 5, no. 1, p. 10148, May 2015.

[17] Q. Li, W. Li, J. Zhu, L. Zhang, and Y. Liu, "Implementing orbital angular momentum modes using single-fed rectangular patch antenna," *Int. J. RF Microwave Comput.-Aided Eng.*, vol. 30, pp. –5, May 2020, Art. no. e22165.

[18] W. Li, L. Zhang, S. Yang, K. Zhuo, L. Ye, and Q. H. Liu, "A reconfigurable second-order OAM patch antenna with simple structure," *IEEE Antennas Wireless Propag. Lett.*, vol. 19, pp. 1531–1535, 2020.

[19] Z. K. Meng, Y. Shi, W. Y. Wei, and X. F. Zhang, "Multifunctional scattering antenna array design for orbital angular momentum vortex wave and RCS reduction," *IEEE Access*, vol. 8, pp. 109289–109296, 2020.

[20] Y.-Y. Wang, Y.-X. Du, L. Qin, and B.-S. Li, "An electronically mode reconfigurable orbital angular momentum array antenna," *IEEE Access*, vol. 6, pp. 64603–64610, 2018.

[21] D. Liu, L. Gui, Z. Zhang, H. Chen, G. Song, and T. Jiang, "Multiplexed OAM wave communication with two-OAM-mode antenna systems," *IEEE Access*, vol. 7, pp. 4160–4166, 2019.

[22] L. Gui, M. R. Akram, D. Liu, C. Zhou, Z. Zhang, and Q. Li, "Circular slot antenna systems for OAM waves generation," *IEEE Antennas Wireless Propag. Lett.*, vol. 16, pp. 1443–1446, 2017.

[23] W. J. Byun, K. S. Kim, B. S. Kim, Y. S. Lee, M. S. Song, H. D. Choi, and Y. H. Cho, "Multiplexed Cassegrain reflector antenna for simultaneous generation of three orbital angular momentum (OAM) modes," *Sci. Rep.*, vol. 6, no. 1, p. 27339, Jun. 2016.

[24] Z.-G. Guo and G.-M. Yang, "Radial uniform circular antenna array for dual-mode OAM communication," *IEEE Antennas Wireless Propag. Lett.*, vol. 16, pp. 404–407, 2017.

[25] D. Liu, L. Gui, K. Chen, L. Lang, Z. Zhang, H. Chen, L. Liu, and T. Jiang, "Theoretical analysis and comparison of OAM waves generated by three kinds of antenna array," *Digit. Commun. Netw.*, vol. 7, no. 1, pp. 16–28, Feb. 2021.

[26] S. M. Mohammadi, L. K. S. Daldorff, J. E. S. Bergman, R. L. Karlsson, B. Thide, K. Forozesh, T. D. Carozzi, and B. Isham, "Orbital angular momentum in radio—A system study," *IEEE Trans. Antennas Propag.*, vol. 58, no. 2, pp. 565–572, Feb. 2010.
[27] S. M. Mohammadi, L. K. S. Daldorff, K. Forozesh, B. Thidé, J. E. S. Bergman, B. Isham, R. Karlsson, and T. D. Carozzi, "Orbital angular momentum in radio: Measurement methods," *Radio Sci.*, vol. 45, no. 4, pp. 1–14, Aug. 2010.

DANDAN LIU received the B.S. degree from Xidian University, Xi'an, China, in 2013, and the Ph.D. degree from the School of Electronic Information and Communications, Huazhong University of Science and Technology (HUST), Wuhan, in 2020.

She has been a Lecturer with the College of Weapons Engineering, Naval University of Engineering, Wuhan, China, since September 2020. Her research interests include wireless communication, radar detecting, antenna design, and OAM waves.

QINQIN SUN received the B.S. degree from Anhui University of Technology, Ma'anshan, China, in 2013, and the M.S. degree from the School of Electronic Information and Communications, Huazhong University of Science and Technology (HUST), Wuhan, in 2015.

He is currently an Engineer with Wuhan Maritime Communication Research Institute, Wuhan, China. His research interests include wireless communication and software radio.

WEI WU was born in Hubei, China, in 1981. He received the B.S., M.S., and Ph.D. degrees from Naval Aeronautical and Astronautical University, Yantai, China, in 2004, 2007, and 2011, respectively. He is currently an Associate Professor with the College of Weaponry Engineering, Naval University of Engineering, Wuhan, China. His current research interests include near space hypersonic target detection and tracking, data fusion, sensor management, and terminal guidance.